Int. J. Wildland Fire 6(4): 177-190, 1996

A Coupled Atmosphere-Fire Model: Role of the Convective Froude Number and Dynamic Fingering at the Fireline

Terry L. Clark[1], Mary Ann Jenkins[2], Janice L. Coen[1], and David R. Packham[3]

[1]Mesoscale and Microscale Meteorology Division National Center for Atmospheric Research, P.O Box 3000 Boulder, Colorado 80307-3000, USA*
Tel. 1 303 497 8978; Fax 1 303 497 8181; email clark@ncar.ucar.edu

[2]149 Petrie Science Building Department of Earth and Atmospheric Science York University, 4700 Keele Street North York, Ontario, M3J 1P3, Canada

[3]Department of Geography and Environmental Sciences Monash University Clayton, Victoria 3186, Australia

Abstract. A numerical atmospheric model is coupled with a simple dry eucalyptus forest fire model to create a wildfire simulation model. This is used to show how certain atmospheric conditions can lead to commonly observed forest fire behavior. Using short line fires, simulations show that with moderate winds, the fire line interacts with the updraft ahead of it causing the fire line to curve forward into a conical shape. Other experiments show that when ambient winds change with height, a pair of rotating updrafts at the curved fire front can touch down within the fire and break up the fire line. We also demonstrate 'dynamic fingering', in which the rotating columns near the fire front intensify to tornado strength and can result in rapid and strong increases in the fire spread rate.

Keywords: Fire dynamics; Atmospheric model; Dynamic fingering

Introduction

Until recently, studies on the effects of forest fires on the atmosphere have treated the fire-atmosphere as an uncoupled system. For example, recent modeling studies by Heilman and Fast (1992), and Heilman (1992), investigating the intense heating effects in wildfires, used a two-dimensional, non-hydrostatic model with terrain-following coordinates, but did not include coupling between fire and dynamics. Recent exceptions in fire modeling are the works of Grishin (1992) and the most recent work of Clark et al. (1996), hereafter referred to as CJCP. These works point to the serious need to consider coupling between the fire and the atmospheric dynamics because the energy released by an intense fire is strong enough to drive the atmospheric dynamics over a wide range of spatial scales.

*The National Center for Atmospheric Research is sponsored by the National Science Foundation.

Forest fires produce extremely strong vortices as evidenced by Banta et al. (1992) in their remote sensing of two forest fires and even in much less intense experimental fires (Church et al.; 1980). The main sources of vorticity are horizontal gradients in buoyancy and surface friction. Rotors produced by these two sources can be tilted and/or amplified by stretching. Another source is the solenoidal effect which results from the cross product between the gradients of density and pressure. Usually this source is neglected in small scale modeling although with the presence of strong gradients of buoyancy resulting from the fire its effect should be evaluated. The analysis by CJCP and subsequent simulations (not shown) indicate its effect is negligible for all simulations performed to date. Capturing all significant sources of vorticity is essential in coupled fire-atmosphere modeling in order to realistically assess the effect of coupling.

CJCP have taken a three-dimensional mesoscale model — which has been used successfully on a wide variety of meteorological phenomena such as downslope windstorms, severe cumulus convection, frontal dynamics and tropical convection — and coupled it with a simple dry eucalyptus forest fire model to establish a time-dependent wildfire simulation model. This paper is a continuation of their work where the same model addresses further questions regarding the energetics and some nonlinear processes associated with atmosphere-fire dynamics.

CJCP present coupled simulations of straight-line forest fires demonstrating how the location and structure of the low-level convection pattern feeds back on the fireline dynamics to induce a parabolic or cone-like shape to the evolving fire line in constant ambient wind conditions. They show that if the wind speed is strong enough to force the convection column of hot air to lie close in front of the fire line, then the projection of the low-level convergence pattern onto a straight-line fire results in a bell-shaped rate of spread. Figure 1 shows a short line fire (420 m) in a

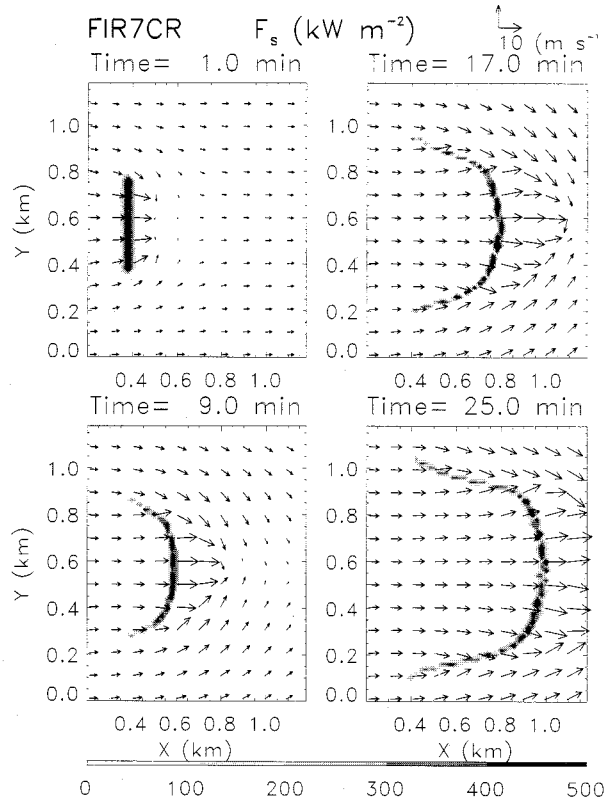

Figure 1. Four time levels of fire-line evolution of surface fuel ignition in a constant ambient wind of $U_0 = 3\ m\ s^{-1}$ for experiment FIR7CR. Shaded regions indicate fire fluxes in kW m^{-2}. The initial fire length is 420 m.

constant 3m s^{-1} mean wind. Here the updraft of the buoyant column of hot air lies just in front of the fire. As a result, the buoyant column draws air (normal to the fire line) much faster from the center of the fire than from its sides and the fire line quickly evolves a pronounced parabolic shape. If the wind speed is too strong, then the convection column is too far removed from the fire to allow any interaction. CJCP also show that this same mechanism can explain the multiple protrusions (or fingers) that are observed to develop in much longer wind-driven fires such as the 1987 Onion fire in the Owens valley (Charles W. George, USDA Forest Service, personal communication). The protrusions in this case aligned with the wind and were spaced about 1 km apart. The added complexity here is that, when buoyant updrafts become long enough, instabilities in the atmospheric dynamics cause them to break into multiple convection columns, that eventually induce multiple protrusions or what CJCP call "convective fingers" in the fire line.

CJCP also argue that for their idealized mean-flow conditions increasing the wind strength above some threshold value results in a decreased level of coupling between the atmospheric and fire dynamics. Their argument is based on the square of a convective Froude number

$$F_c^2 = \frac{(U - S_f)^2}{g \frac{\langle \Delta\theta \rangle}{\langle \theta \rangle} W_f}, \qquad (1)$$

which provides a measure of the ratio of the kinetic energy of the air (relative to the fire) over the sensible[1] heat flux provided by the fire. Byram (1973) and Grishin (1992) present similar Froude numbers to characterize fire behavior. U and S_f represent the wind speed and rate of fire spread, W_f is the width of the fire, $\Delta\theta/\bar{\theta}$ the convective buoyancy, and g gravity. An advantage of a quantitative model like CJCP's is that important controlling parameters such as F_c^2 can be explicitly calculated over a wide range of conditions and its utility tested. For large wind speeds and corresponding large F_c^2 values, air parcels remain in the fire for such a short period of time that atmosphere-fire dynamic interactions are negligible. However, for small wind speeds and F_c^2 values, the air and fire should be strongly coupled. This latter condition we believe is where coupled atmosphere-fire modeling can make important contributions. For example, we discuss in Section 4 that a small F_c^2 may be a necessary condition for a blowup fire to occur. [According to Byram (1954), a blowup fire is one which suddenly, and often unexpectedly, multiplies its rate of energy output many times, sometimes in a matter of min. The blowup fire can be large or small, but is extremely dangerous to fire fighters.] We hypothesize that blowups result from a bifurcation in F_c^2 space due to an extreme level of interaction between the atmospheric and fire dynamics. We plan to test this hypothesis in the future.

In CJCP the background wind speeds are constant for each experiment and range between 1 to 5 m s^{-1}, too small a variation in speed to clearly demonstrate the critical values of F_c^2 or their utility. In the present paper we show results with constant background winds, U_0, ranging from 1 to 20 m s^{-1}, more than adequate to span the parameter space of strong and weak coupling. These experiments are also used to test CJCP's hypothesis that, for the present model formulation, strong wind conditions lead to rapidly spreading but dynamically stable forest fires. Such results are important if we are to develop a good understanding of the dynamics leading to and causing blowups.

Figure 2 shows a schematic of a process CJCP refers to as "dynamic fingering", one specific type of small-scale dynamical process occurring at fire fronts that may affect strong feedbacks between the atmosphere and fire dynamics. Figure 2 illustrates how the vertical tilting of regions of intense horizontal negative shear (i.e., winds decreasing with height) at the fire front lead to narrow regions of high speed, hot air shooting out in front of the fire. What the figure shows is that the low level wind shear can be

[1]Sensible heat is the energy measured by temperature.

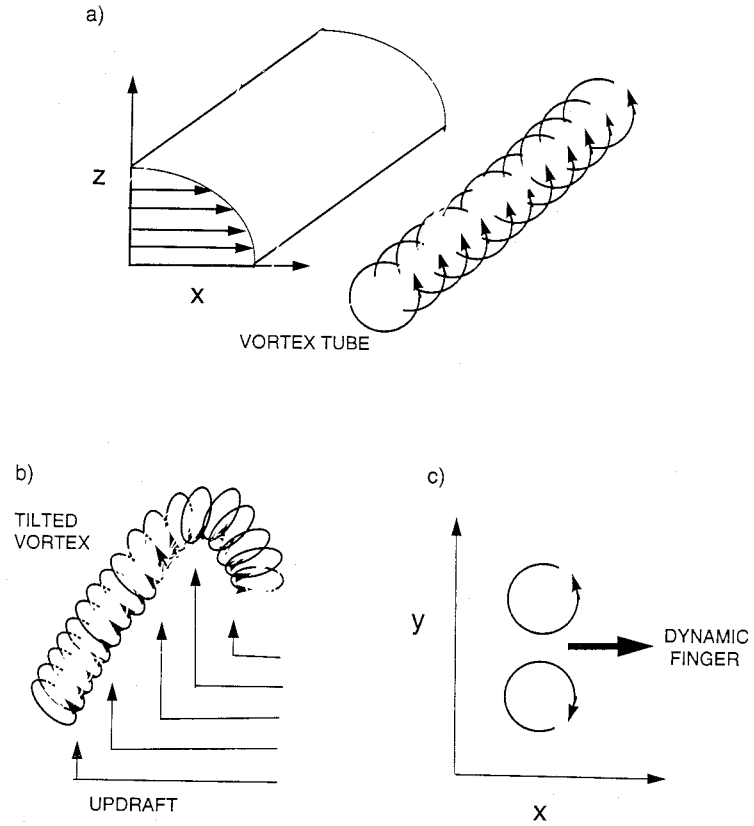

Figure 2. The vortex dynamics associated with "dynamic fingering". See text for explanation.

viewed as rotating flow. When this flow is vertically tilted by localized updrafts it results in bending this ribbon of vorticity (or rotating flow) into the vertical. As the sides of the ribbon approach each other this leads to enhanced local winds as shown in the down-looking lower right plane view. We refer to these narrow regions as fingers; thus the term "dynamic fingering". It is hypothesized that these small-scale fingers of hot gas may cause the rate of fire spread to increase dramatically. Dynamic fingering may represent a major process in fire spread on the microscale which causes fires to "jump" as they spread. This is a strongly nonlinear process occurring on scales of tens of meters and has little relationship to the convective type of fingering described in detail by CJCP that affects the overall fire shape. "Convective fingering " is a process that occurs on much larger scales and involves atmospheric dynamics that are essentially linear.

Probably a necessary, but not sufficient, condition for dynamic fingering to occur is that F_c^2 be small, i.e., the atmosphere-fire dynamics must be strongly coupled before any fire front vortices that are tilted can be near the fire. Our simulations to date suggest that even when the value of F_c^2 indicates strong coupling, fire-line dynamics remain stable, showing little dynamic fingering activity. This indicates that something besides small F_c^2 is needed before dynamic fingering can occur. Figure 2 suggests that a likely candidate is low-level shear. Byram (1954) noted that a common feature of blowup fires is the presence of low-level negative shear where the wind blows faster near the surface than just aloft. There are numerous ways of producing low-level shear in the ventilation pattern of the fire. These include gust fronts, convective downdrafts and mountain valley flows. In the present paper we rely on a longer term integration to produce convective motions that provide a variety of eddies in the boundary layer. A single dynamic fingering event is obtained with this procedure and is discussed in Section 4. It is associated with a convective downdraft that propagated into the ventilation region and interacted with the fire. This weak dynamic fingering event is also accompanied with the intensification of a pre-existing strong whirlwind of tornado strength that is produced by the fire front dynamics.

Model Description

Here we describe the components of the model used in this study, including the governing equations of the atmospheric model and the current fire model.

The continuity and momentum equations of the mesoscale model

Using mixed vector and tensor notation, the momentum equations of the atmospheric model are

$$\bar{\rho}\,\frac{d\vec{V}}{dt} = -\nabla p' + g\bar{\rho}B + \frac{\partial \tau_{ij}}{\partial x_j} \qquad (2)$$

and the anelastic continuity equation is

$$\nabla \cdot \bar{\rho}\vec{V} = 0. \qquad (3)$$

Here $\vec{V} = (u\hat{\mathbf{i}}, v\hat{\mathbf{j}}, w\hat{\mathbf{k}})$ is the air's velocity in the x, y, and z Cartesian coordinate system, $\bar{\rho} = \rho(z)$ the base state air density, p' and B the respective perturbation pressure and buoyancy, and τ_{ij} the stress tensor. The d/dt is the Lagrangian time t derivative, ∇ the three-dimensional gradient operator. The τ_{ij} stress terms are treated using a first-order subgrid closure (Smagorinsky, 1963; Lilly, 1962) with a near-surface Blackadar (1962) grid-scale with a surface roughness height, z_0, drag formulation.

The buoyancy is approximated in biconstituent form (Schaefer, 1975) as

$$B = \left(\frac{\theta'}{\theta}(1+\epsilon q_v) + \epsilon q_v - q_c - q_r\right), \qquad (4)$$

where q_v, q_c, and q_r represent the mixing ratios of water vapor, cloud water, and rain water, respectively. Here θ is potential temperature and the constant $\epsilon = 0.622$. The primes denote a deviation from a horizontal average.

The solenoidal effect, Coriolis force, mountainous terrain, and canopy drag are all neglected in the present paper, although the model is formulated to treat both Coriolis, solenoidal effects and mountainous terrain. The cloud physics are approximated using the warm rain parameterization of Kessler (1969). The ice physics of the model are turned off.

The thermodynamic equation of the mesoscale model

The conservation equation for a thermodynamic variable ψ (which represents any of θ, q_v, q_c or q_r) is

$$\frac{\partial}{\partial t}\bar{\rho}\psi + \nabla \cdot (\bar{\rho}\vec{V}\psi) = S_\psi + \frac{\partial}{\partial x_i} H_i^\psi, \qquad (5)$$

where S_ψ is the local grid scale and H_i^ψ the subgrid flux of ψ in the x_i direction. The $\partial/\partial t$ operator is the local time change. Sensible and latent[2] heat fluxes associated with the fire are introduced into the atmospheric model by modifying the vertical fluxes H_3^θ and $H_3^{q_v}$ as

$$H_3^\theta = \bar{\rho}K_H\frac{\partial \theta}{\partial z} + F_s(\vec{x},t) \qquad (6)$$

and

$$H_3^{q_v} = \bar{\rho}K_H\frac{\partial q_v}{\partial z} + F_l(\vec{x},t) \qquad (7)$$

where K_H is the coefficient of eddy thermal diffusion and F_s and F_l are the sensible and latent heat fluxes.

The fire model

The fire model is extremely simple, designed as a test bed with which to evaluate the potential utility of a coupled mesoscale atmosphere-fire model, and will undergo significant improvements in the future. The fire's fuel characteristics are treated as a homogeneous dry eucalyptus forest with both ground and canopy fuel. Ground and canopy fuels are specified in units of kg m^{-2}. Following Walker (1981), the initial mass of the ground fuel is 2.7 kg m^{-2} which is comprised of 2.0, 0.5, and 0.2 kg m^{-2} of ground litter, trash, and scrub, respectively. The litter, trash, and scrub are assigned burn rates of 0.040, 0.005, and 0.004 kg m^{-2} s^{-1}, respectively. The initial dry mass of the forest canopy is 1.2 kg m^{-2} with an initial moist/dry ratio of 1.25. The burn rate of the dry canopy fuel is 0.020 kg m^{-2} s^{-1}. The combustion coefficient of 1.7 x 10^7 J kg^{-1} is applied to each dry fuel type. As part of the description of the fuel (Walker; 1981), 3% of the sensible heat released is used to evaporate water contained in the ground fuel. Also, the chemical equation governing the combustion of cellulose results in the conversion of 56% of the dry fuel's mass to water vapor.

To emulate smoldering, the burn rates are premultiplied by B_{ratio} which both limits the rate for slow fire velocities and adds a random component. The formula for B_{ratio} is

$$B_{ratio} = \sqrt{\frac{(|\vec{V}_h| + 1.)}{(|\vec{V}_h| + 4.)}}\, r_f, \qquad (8)$$

where the units for each term under the square root are m s^{-1}, $|\vec{V}_h|$ is the fire spread-rate, and r_f is a random factor that varies between 1±0.05 that is added to quickly excite

[2]Latent heat is the energy released by condensation of water vapor.

dynamic instabilities that might be present. The terms under the square root in (8) are added as a crude means of accounting for O_2 oxygen limitation. This portion of (8) will be dropped in the future as it really is not a good approximation of O_2 depletion. Fortunately, its inclusion had little effect on the results.

Fuel is divided into rectangular grids and is ignited by contact only. Four tracers are assigned to a grid cell once the ground fuel for that particular cell is ignited. The tracers are free to move in any direction and are not confined by the rectangular geometry of the fuel. Based on the following empirical McArthur formula for fire spread-rate S_f (Noble et al., 1980), the tracers move parallel with and against, and normal right and left of, the wind. Tracers normal to the wind $\vec{V}_h$ move at speed S_n, against the wind at speed S_b, and with the wind at speed S_f, where

$$S_n = S_b = 0.18 \text{ m s}^{-1} \tag{9}$$

$$S_f = \begin{cases} S_n \exp(.08424|\vec{V}_h|) & \text{if } S_f \le |\vec{V}_h| \\ |\vec{V}_h| & \text{otherwise.} \end{cases}$$

The tracer-advecting wind, $\vec{V}_h$, and therefore fire speed, S_f, are at the prescribed vertical height of h_{sp} = 15 m above ground level, which represents the top of the canopy. Once a ground tracer reaches an unburned grid box, the burn flag for this new region is then changed from 0 to 1 and four new tracers are initiated at the point of contact. Tracers are not allowed to move into burned out or burning grid boxes.

In the current formulation, the heat flux from the ground fire first goes into drying the canopy. Once the canopy fuel is dry and the ground heat flux exceeds the threshold value of 170 kJ m^{-2}, the canopy ignites. This choice of threshold combined with our choice of fuel types makes all the present simulated fires crown fires. The drying of the canopy will eventually be accounted for by radiation and convection treatments. Although a low intensity ground fire can exist without igniting a crown fire, in the current formulation of the model, a crown fire always co-exists with a ground fire.

The effects of radiation and small scale turbulence heating and moistening the air are parameterized using a simple extinction depth formulation where the vertical structure of the heat fluxes are taken as

$$F_s(\vec{x},t) = F_s(x,y,0,t)\exp(-\frac{z}{\alpha})$$

and

$$F_l(\vec{x},t) = F_l(x,y,0,t)\exp(-\frac{z}{\alpha}), \tag{10}$$

where α = 50 m in the present simulations.

Description of Experiments

The basic experiments of the paper are described in Table 1. For the standard experiment, the mean atmospheric wind, $U(z)$, is set to the constant U_0 at all height levels where U_0 is either 1, 2, 3, 4, 5, 10, 15, or 20 m s^{-1}. The static stability of the atmosphere is prescribed using the Brunt-Väisälä frequency, $N = d\ln\theta/dz$. N =0 for the first 1 km AGL (above ground level), 0.01 s^{-1} for 1 km $< z <$ 10 km, and 0.02 s^{-1} for $z >$ 10km, which represents the stratosphere. The initial atmospheric water vapor mixing ratio, q_v, is set at 12.0 g kg^{-1} throughout the boundary layer[3] and exponentially damped above the boundary layer with an e-folding depth of 400 m, but is not allowed to decay below 0.1 g kg.

The sensible and latent heat released from the burning fuel is enough to initiate cumulus clouds in all the experiments. Cloud base forms near 2.5 km AGL or 1.5 km above the top of the boundary layer. The clouds are shallow and appear to have little direct influence on the fire front dynamics particularly for the experiments using $U(z)$ equal to the constant U_0 as the convection produced by the fire propagates downstream of the fire. However, we did consider one experiment, FR7CS1, where we set the background wind

$$U(z) = 3 - 3[1. + \tanh(\frac{z - 500}{100})] \tag{11}$$

such that $U(z)$ varies from 3 m s^{-1} near the ground, changes sign at z = 500 m, and is asymptotic to -3 m s^{-1} aloft. This hyperbolic tangent profile of $U(z)$ allows the small-scale motions produced by the fire and by the cumulus clouds to propagate upstream of the fire and enter the boundary layer flow that ventilates the fire. Comparisons between FIR7CR and FR7CS1 show the long term effect of these feedbacks.

Three variations on fire-line dynamics are considered. The standard experiment starts with a single 420 m long fire line. Some of the earlier experiments discussed in CJCP erroneously introduced a backfire, and some of these experiments are again considered here as they have the advantage of easily producing convectively disturbed flow in the boundary layer ventilation flow and affecting the fire-line dynamics. A final variation (FIR7E2, see Table 1) is to set two fire lines, both oriented normal to the wind and spaced 400 m apart. The purpose of this experiment is to observe the effect of halving the F_c^2 by doubling the heat flux from the fire for a fixed $U(z)$. Figure 3 shows the variation of F_c^2 with U_0 with locations marked for experiments from Table 1.

[3]The atmosphere-fire coupling does not, as yet, consider fuel moisture adjustments due to atmospheric conditions.

Table 1. Fire experiments and parameters. Initial fire line length for all experiments is 420 m and the height of the fire tracer wind is 15 m AGL.

Experiment	U_0 (m s^{-1})	$U(z)$ profile	Backfire	No. of fire lines	$S_f(U_0)$ (m s^{-1})	$F_c^2(U_0)$	S_{f_a} (m s^{-1})	$F_{c_a}^2$
FIR7AR	1.	const	no	1	0.20	0.025	0.40	0.0069
FIRE7B	2.	const	no	1	0.21	0.11	0.39	0.051
FIR7CR	3.	const	no	1	0.23	0.25	0.43	0.12
FIRE7C	3.	const	yes	1	0.23	0.25	0.42	0.12
FR7CS1	3.	tanh	no	1	0.23	0.25	—	0.13
FIRE7Z	4.	const	no	1	0.25	0.43	0.46	0.21
FIR7DR	5.	const	no	1	0.27	0.62	0.47	0.33
FIRE7E	10.	const	no	1	0.42	1.7	0.56	1.2
FIR7E2	10.	const	no	2*	0.42	0.85	0.70	0.47
FIRE7F	15.	const	no	1	0.64	2.5	0.72	2.2
FIRE7G	20.	const	no	1	0.97	2.9	1.04	2.6

* Fire lines are separated by 400 m.

U_0 = ambient wind speed

S_f = fire spread rate, calculated analytically using (9) with $|\vec{V}_h| = U_0$

F_c^2 = the square of the convective Froude number, given by (1)

S_{f_a} = actual fire speed due to fire front dynamics

$F_{c_a}^2$ = the square of the actual convective Froude number, calculated using

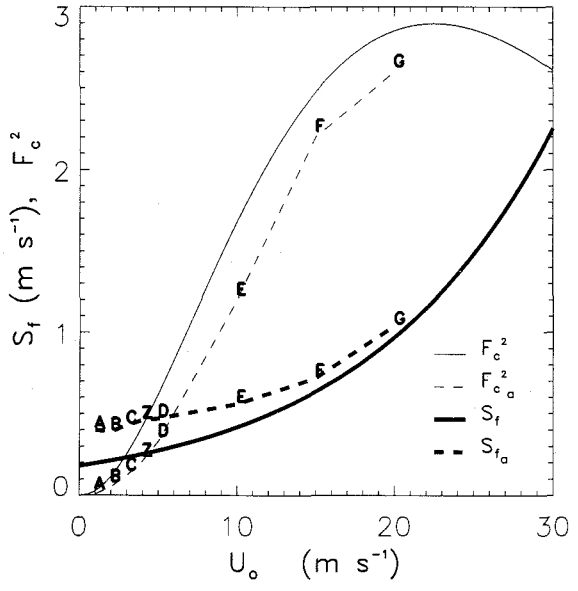

Figure 3. F_c^2 and $F_{c_a}^2$ from (1) and S_f and S_{f_a} from (9) in m s^{-1} as a function of constant background wind U_0. Positions are marked for U_0 = 1, 2, 3, 4, 5, 10, 15 and 20 m s^{-1} corresponding to experiments (Table 1) FIR7AR, FIRE7B, FIR7CR, FIRE7Z, FIR7DR, FIRE7E, FIRE7F, FIRE7G, respectively. Here 6.0 m s^{-1} is a moderate breeze, 12 m s^{-1} a strong breeze, 18 m s^{-1} a gale, 24 m s^{-1} a strong gale, and 30 m s^{-1} a storm. Typical tornadic and mountain downslope winds reach 65 m s^{-1}.

In Figure 3, S_f is the fire spread rate calculated using (9) with $|\vec{V}_h| = U_0$, while S_{f_a} is the "actual" value that occurred in the experiment due to fire front dynamics and $F_{c_a}^2$ the convective Froude number calculated using S_{f_a} in (1). Figure 3 shows that U_0 is not a good estimate of u at the fire front, especially for small U_0 and underestimates actual fire spread rates for $U_0 < 20$ m s^{-1}. As a result, actual $F_{c_a}^2$ values are lower than F_c^2 values. The reason for showing $F_{c_a}^2$ was to demonstrate convergence with F_c^2 with increasing U_0. F_c^2 remains the only operative parameter as it is unambiguous since it is based on ambient flow conditions.

Results

Next, we describe how several factors affected fire dynamics. These include the presence of a backfire, the square of the convective Froude number F_c^2, long-term feedback of the fire-induced circulations on the fire, and the occurrence of a dynamic fingering event.

Effect of backfire on short-line experiments

Table 1 shows that the difference between experiments FIRE7C and FIR7CR is that FIRE7C has a backfire whereas FIR7CR does not. The backfire in FIRE7C is the result of fire tracers directed normal to the wind erroneously moving upwind at the speed of S_n = .18 m s^{-1}. Both experiments experience an initial convective adjustment time of ≈ 1 min before convection is in balance with its heat source. A main physical difference between these two simulations is that the forward moving fire in FIRE7C

is excited by the convective eddies generated by the backfire. The result of this is seen in Figure 4, a plot of fire spread-rates S_f versus time t for FIRE7C and FIR7CR, where the turbulent forcing by backfire eddies produces significant variability in S_f for FIRE7C. If the region of burned out fuel behind the main fire becomes sufficiently cool, then convective downdrafts can penetrate closer to the surface to enhance near surface wind speeds. This buildup of low-level shear adds to the instability of the fire front and to the possibility for increased S_f. This is evident at $t \approx 4$ min in FIRE7C when S_f suddenly increases from $\approx$ 0.4 to 0.5 m s^{-1} and then drops back to $\approx$ 0.4 m s^{-1}. Unlike FIRE7C, S_f versus t for FIR7CR (no backfire) is extremely regular, showing a fundamental period of about 45 s with a second harmonic of half this period. This regular period appears to be an artifact of the model resulting from the sudden ignition of the 10 m square grid of fuel every $\Delta x_{fuel}/S_f \approx$ 43 s. The periods for the other experiments show a clear trend of increasing frequency and decreasing amplitude with increasing U_0, supporting the above hypothesis.

It is also possible that the backfire preheats air coming into the fire, reducing low-level wind speeds and wind shear to, in effect, stabilize the fire by reducing the effective $\Delta\theta$ and increasing F_c^2. Figure 4 shows that after the initial convective adjustment time, and other than the peak at $\approx$ 4 min, the maximum S_f for FIRE7C (backfire) remains temporally fairly uniform, while for FIR7CR (no backfire) the maximum S_f steadily increases with time.

Effect of F_c^2 on flow pattern

Figure 5 shows vertical cross sections of temperature anomaly through the middle of the fire line for U_0= 1, 3, 4, 5, 10, and 15 m s^{-1} at t = 6 min. As U_0 increases the wind tends to flow through the fire, while the air shows little vertical deflection. This is particularly noticeable for $U_0 >$ 5 m s^{-1}where the coupling between the fire and the atmospheric dynamics is weak ($F_c^2 > 0.6$). Another characteristic demonstrating the decoupling with increasing U_0 is seen in Figure 6. For the same experiments as Figure 5 and t = 6 min, Figure 6 shows that when U_0= 10 and 15 m s^{-1}, the shape of the central portion of each fire line has stayed linear, i.e. for $U_0 >$ 5 m s^{-1}, the near surface convergence pattern of the convection column is decoupled from the fire.

Figures 7 and 8 show cross sections of vertical velocity $w(x,y)$ and $w(x,z)$, respectively, for the same cases and

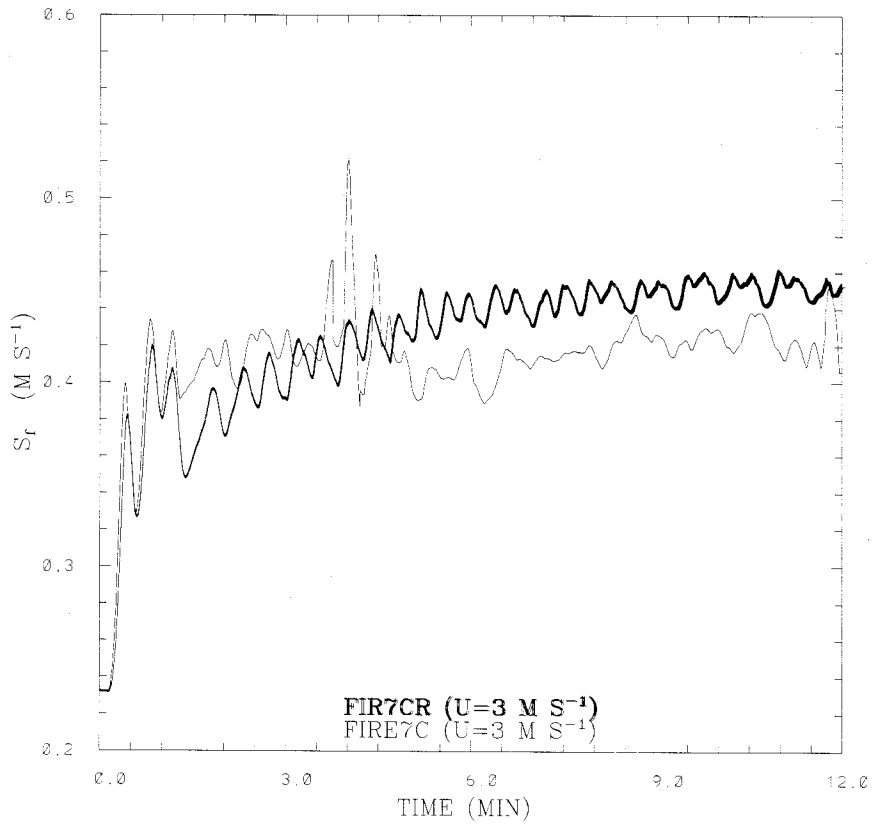

Figure 4. Maximum rate-of-fire spread $S_{f_{max}}$ in m s^{-1} versus time t in min for experiments FIRE7C (backfire) and FIR7CR (no backfire) in a constant ambient wind of U_0 = 3 m s^{-1}

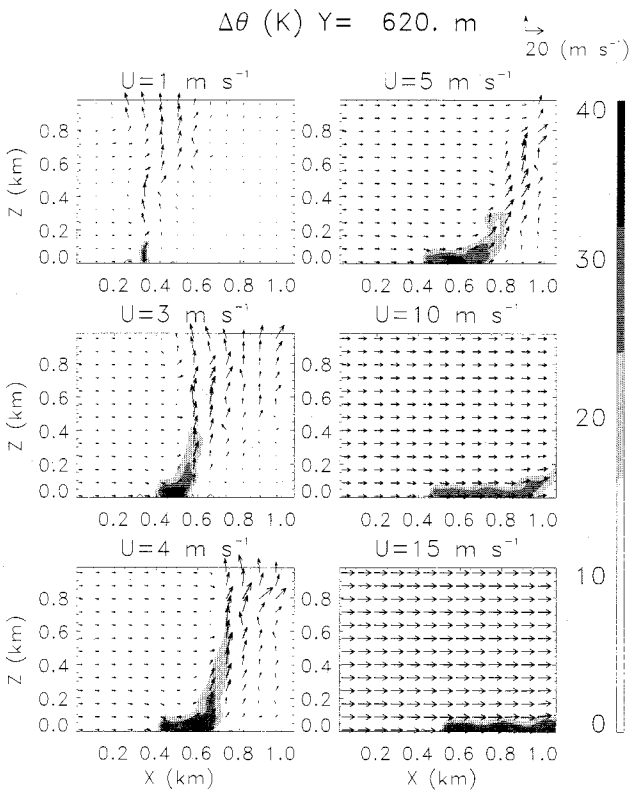

Figure 5. Vertical cross sections of temperature anomaly $\Delta\theta(x,z)$ for U_0 = 1, 3, 4, 5, 10, and 15 m s^{-1} at t = 6 min corresponding to experiments FIR7AR, FIR7CR, FIRE7Z, FIR7DR, FIRE7E, and FIRE7F, respectively. The corresponding value of U_0 is noted above each plate. The cross sections are aligned in the mean wind direction through the center of the fire line at y = 620 m. Arrows represent wind vectors.

times as Figures 5 and 6. As U_0 increases in Figure 7, the maximum updraft moves ahead of the fire and decreases in magnitude, giving the decoupling noted in Figures 5 and 6. It is evident in Figure 8, at least within this limited domain, that both the magnitude and vertical extent of the fire decrease with increasing U_0.

As a test of F_c^2, we ran the case FIR7E2 with U_0 = 10 m s^{-1} and two fire lines initially spaced 400 m apart in the direction of the mean wind (F_c^2 = 0.85). By doubling the heat source in FIR7E2, we might expect it to resemble FIR7DR (U_0 = 5 m s^{-1}, single line fire, F_c^2 = 0.65) more than than FIRE7E (U_0= 10 m s^{-1}, single line fire, F_c^2 = 1.7) if the dominant parameter is F_c^2.

Although convection in FIR7E2 is initiated by two parallel fire lines, the forward fire plume entrains the rear one and becomes a single plume. Plume studies by Rouse, Baines and Humphreys (1953) show that two plumes initiated by two parallel line sources in a zero ambient wind entrain each other and become a single plume located midway between the sources which behaves as though a single line source was located beneath it. In this case, Figure 9 shows that by t = 2 min the fire plume behaves as though a single line source is located beneath it and the source is essentially collocated with the forward line fire.

In the double fire line experiment FIR7E2, the front fire moves much faster than in the single fire line experiment FIRE7E (S_{fa} = 0.70 m s^{-1} compared to S_{fa} = 0.56 m s^{-1}). Based on the square of the actual convective Froude numbers, the coupling between the fire and the atmospheric dynamics is also much greater in FIR7E2 (F_c^2 = 0.62) than in FIRE7E (F_c^2 = 1.7), where, as seen in Figures 5 to 8, the coupling is weak. In FIR7E2, the coupling is weak for the rear fire line, significant for the forward fire line. Figure 9 shows little vertical deflection in the air flowing over the rear fire; winds flow through the rear fire and are entrained by the forward, vertically-tilted, fire plume. Figure 10 shows that the shape of the central portion of the rear fire line stays linear, while the forward fire line evolves into a parabolic-like shape. The downstream near-

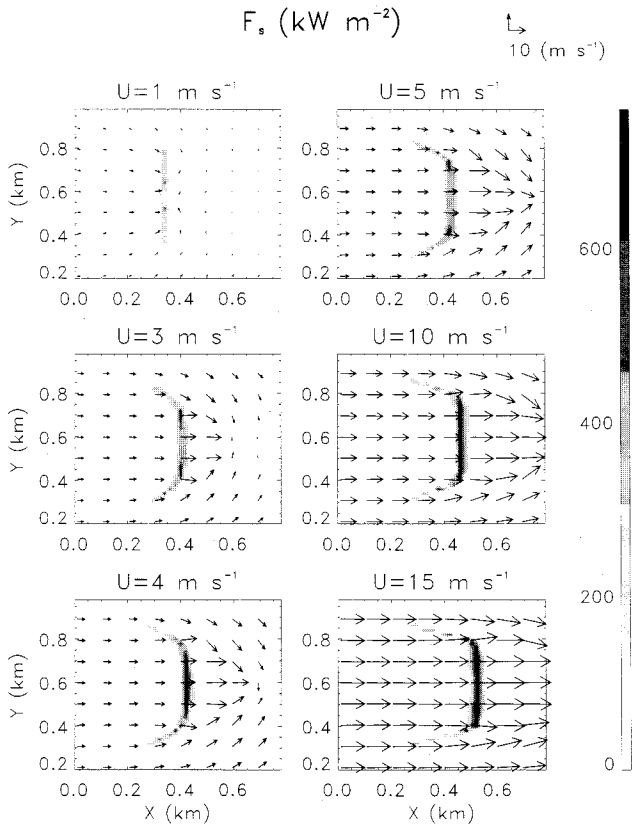

Figure 6. Plots of fire line ignition at t = 6 min for the six cases shown in Figure 5. Shaded regions indicate fire fluxes in kW m^{-2}. The initial fire length is 420 m. Arrows represent wind vectors at 30 m AGL.

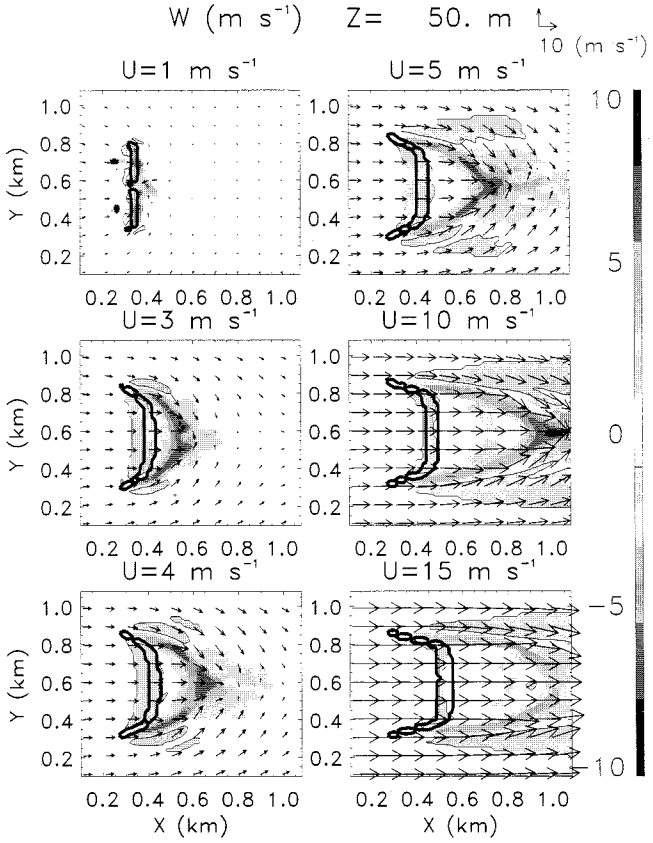

Figure 7. Horizontal cross sections of vertical velocity $w(x,y)$ for U_0 = 1, 3, 4, 5, 10, and 15 m s^{-1} at t = 6 min corresponding to experiments FIR7AR, FIR7CR, FIRE7Z, FIR7DR, FIRE7E, and FIRE7F, respectively. The cross sections are taken at z = 50 m AGL and arrows represent wind vectors taken at 15 m AGL.

surface convergence pattern of the single convective column is coupled with the forward fire (seen clearly in the wind vectors), but this convergence is too far upstream to affect the shape of the rear fire line.

FIR7E2 does resemble FIR7DR more than FIRE7E, demonstrating the significance of the convective Froude number, however there are differences in behavior and structure. In FIR7E2, the fire fronts travel faster (S_{fa} = 0.70 m s^{-1}) than in the single fire line experiment FIR7DR (S_{fa} = 0.48 m $^{-1}$). And, based on the actual convective Froude numbers, the coupling between the fire and the atmosphere is slightly greater for FIR7DR (F_c^2 = 0.62) than FIR7E2 (F_c^2 = 0.85). In FIR7DR, winds are entrained by the fire (Figure 5 shows a small, upright plume at t = 6 min) whereas for FIR7E2, the greater ambient wind case, (Figure 9) there is a single large plume, strongly tilted downstream.

Effect of fire-induced motions on fire evolution

Two experiments were run to demonstrate the effect of long term feedback of the fire-induced convection on the fire. FIR7CR used a constant wind of U_0 = 3 m s^{-1} throughout the atmosphere, whereas FR7CS1 used $U(z)$ set equal to an hyperbolic tangent profile where $U(z)$ is +3 m s^{-1} at the surface z =0, zero at z = 500 m, and asymptotic to -3 m s^{-1} for z >> 500 m. In FIR7CR the convective motions are all advected downstream of the fire since S_f < 3 m s^{-1}. In FR7CS1 the convective motions are eventually advected to the rear of the fire, providing the opportunity to re-enter the fire. Figure 11 shows the time series of $S_{f\,max}(t)$ for these two cases over a period of 28 min. In FIR7CR, $S_{f\,max}$ remains steady at $\simeq$ 0.4 m s^{-1} throughout this period, whereas in FR7CS1 $S_{f\,max}$ displays very nonuniform behavior, departing dramatically from a steady value once t > 15 min, the time required to recycle convective eddies on the scale of the fire. In this case, at t = 24.4 min $S_{f\,max}$ jumps erratically to $\simeq$ 0.9 m s^{-1}. As discussed in the next section, this particular variation in $S_{f\,max}$ corresponds to a dynamic fingering event brought on by the actions of the downdraft of a convective eddy.

Figures 1 and 12 show the evolution of fire ignition for these two cases. We see that while FIR7CR retains its integrity throughout the 28 min integration period,

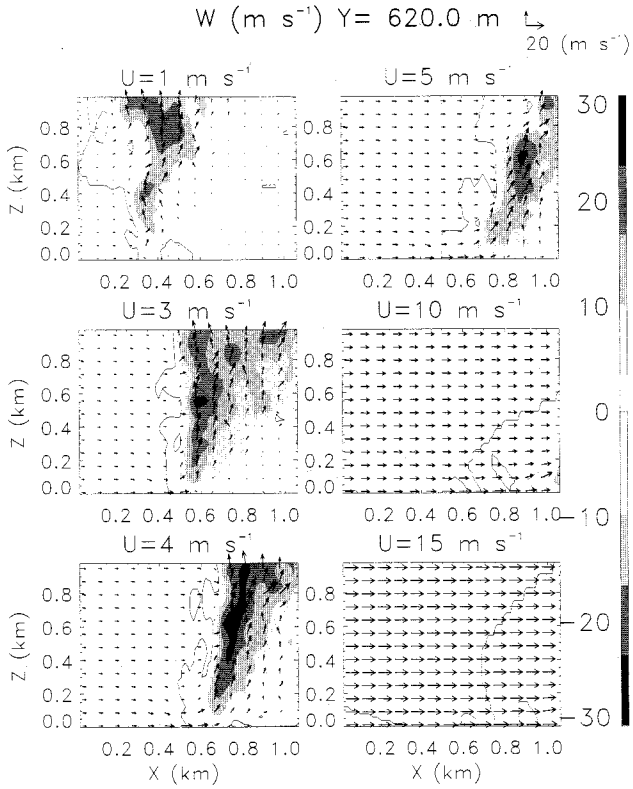

Figure 8. Vertical cross sections of vertical velocity $w(x,z)$ for U_0 = 1, 3, 4, 5, 10, and 15 m s^{-1} at t = 6 min corresponding to experiments FIR7AR, FIR7CR, FIRE7Z, FIR7DR, FIRE7E, and FIRE7F, respectively. The cross sections are aligned in the mean wind direction through the center of the fire line at y = 620 m. Arrows represent wind vectors.

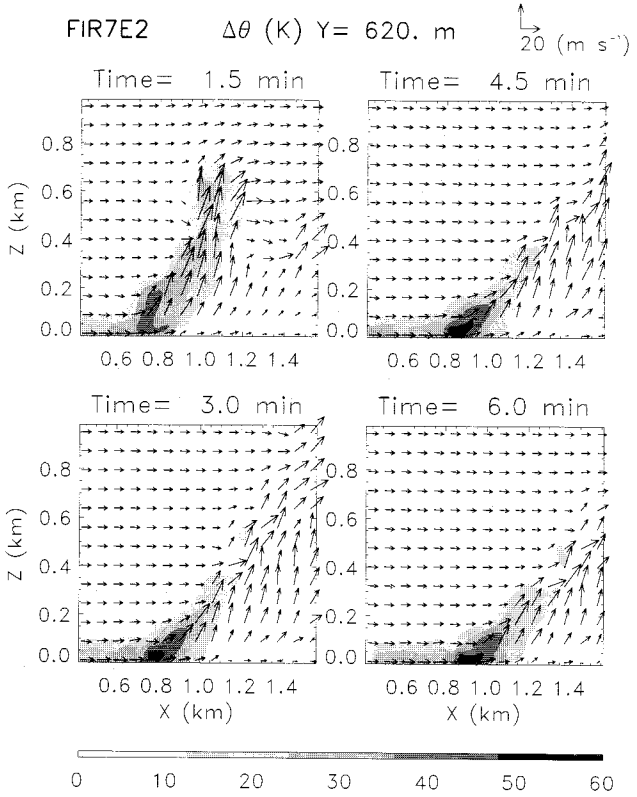

Figure 9. Four time levels of vertical cross sections of temperature anomaly $\Delta\theta(x,z)$ for $U_0 = 10$ m s^{-1} in double fire line experiment FIR7E2. The cross sections are aligned in the mean wind direction through the center of the fire line at $y = 620$ m. Arrows represent wind vectors.

FR7CS1 breaks up by t = 20 min as a result of the feedback of the fire-induced motions. The curved shape of the fire line results in the development of two counter rotating vortices positioned at the point of the fire. The sense of this vortex pair provides rotation that directs air towards the fire at its center. As shown in Figure 13(b), the environment of the hyperbolic tangent wind profile allows this vortex pair to eventually touch down within the fire line in experiment FR7CS1, where the opposing winds from the vortex pair blow air into the fire and break up the fire line. As shown in Figure 13(a), a similar vortex pair is produced that eventually touches down, but well in front of the fire line without strongly affecting the fire line dynamics. This mechanism of fire line break-up is similar to that causing so-called storm splitting in numerical simulations of cumulonimbus clouds (Wilhelmson and Klemp, 1978). Clark (1979) discusses the storm splitting process in the context of cloud modeling as an artifact of the schemes used to initialize the models. However, in the context of forest fires the process appears to be physically well based.

A dynamic fingering event

A single event of dynamic fingering is observed in the north-east sector of the fire front. Figures 14, 15 and 16, show the respective w, $\frac{\partial|\vec{V}|}{\partial z}$, and wind speed $|\vec{V}|$ fields accompanying the event. This particular fingering event is caused by the advection of a fire-induced downdraft into the rear ventilation flow. The downdraft produced a region of near surface vertical shear that moved through the fire front adjacent to an existing vertical rotor. The vertical tilting of this shear by local updrafts intensified the rotation rate of the vertical rotor leading to an anomalous wind speed maximum. The large maximum S_f values shown in Figure 11 for t > 18 min result from this type of forcing. The combination of the effects of local $w, \frac{\partial|\vec{V}|}{\partial z}$ fields in intensifying the rotation rate of the fire vortex is seen in Figure 17 which shows the vorticity source $-\hat{k} \cdot \nabla w \times \frac{\partial \vec{V}}{\partial z}$ due to vortex tilting. Since this is an isolated event in the fire simulations, the amplifica-

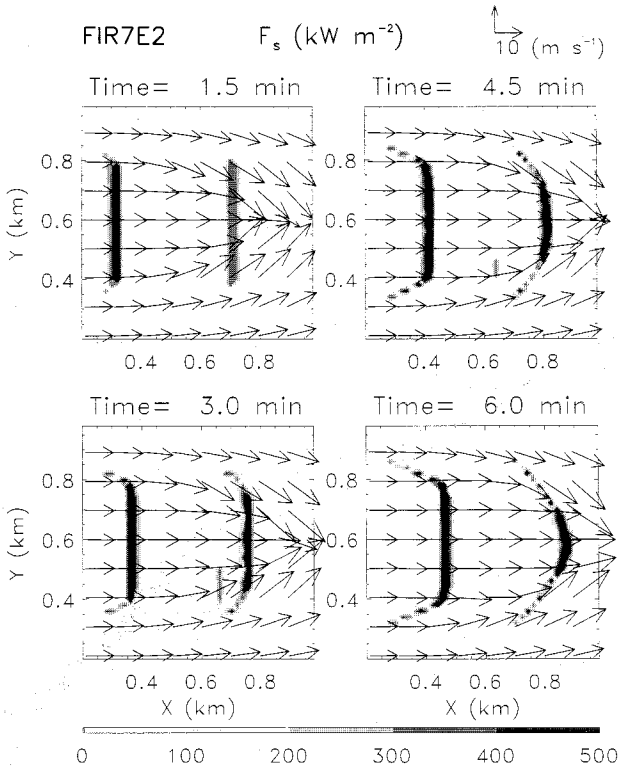

Figure 10. Four time levels of surface fuel ignition in a constant ambient wind of $U_0 = 10$ m s^{-1} in double fire line experiment FIR7E2. Shaded regions indicate fire fluxes in kW m^{-2}. The initial fires are 420 m long and are separated by 400 m. Arrows represent wind vectors taken at 15 m AGL.

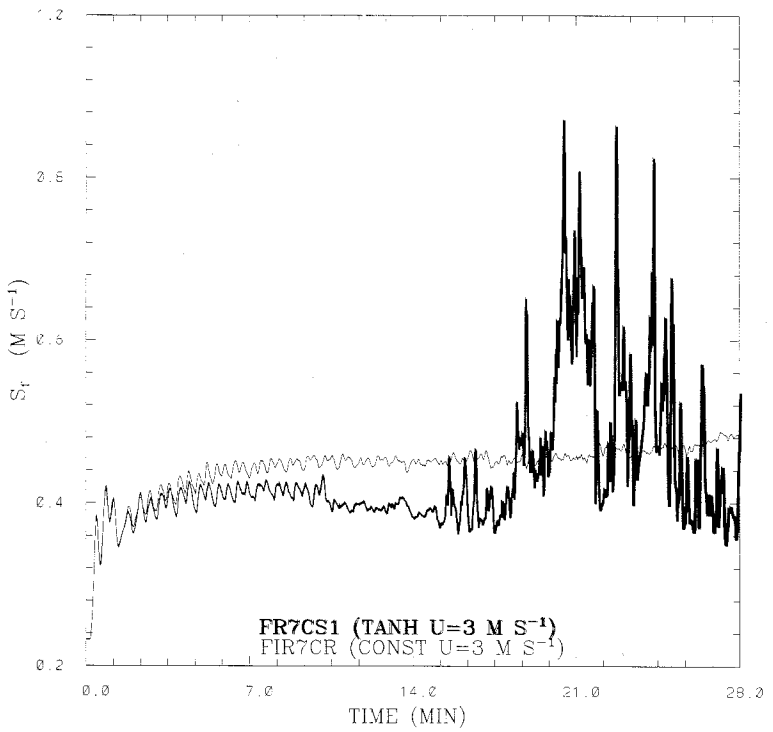

Figure 11. Maximum rate-of-fire spread $S_{f_{max}}$ in m s^{-1} versus time t in min for FIR7CR (constant ambient wind of $U_0 = 3$ m s^{-1}) and FR7CS1 (tanh profile ambient wind of $U_0 = 3$ m s^{-1}).

tion of S_f through dynamic fingering does not lead to runaway fire spread. This type of local vortex dynamics is probably involved in causing fires to jump in some cases as they spread.

Conclusions

Simulations of coupled forest fire and atmospheric dynamics are performed over a range of mean ambient wind speeds to assess the utility of the square of the convective Froude number, F_c^2, in predicting fire line behavior. The experiments use a simple empirical fire model based on the McArthur fire spread meter. The results show that for moderate to low wind speeds the coupling between the fire and the atmosphere is significant, leading to strong feedbacks between the fire induced motions and fire-line spread. This initial study simplifies the coupling by using fire parameters from a dry eucalyptus forest fire applied to an empirical rate-of-spread model. The fire coupling does not, as yet, consider fuel moisture adjustments due to atmospheric variations. This will be considered in later work. Wind speeds of 10 or greater result in faster rates of fire spread, but weaker fire-atmosphere coupling with no noticeable feedback between the fire and fire-induced motions.

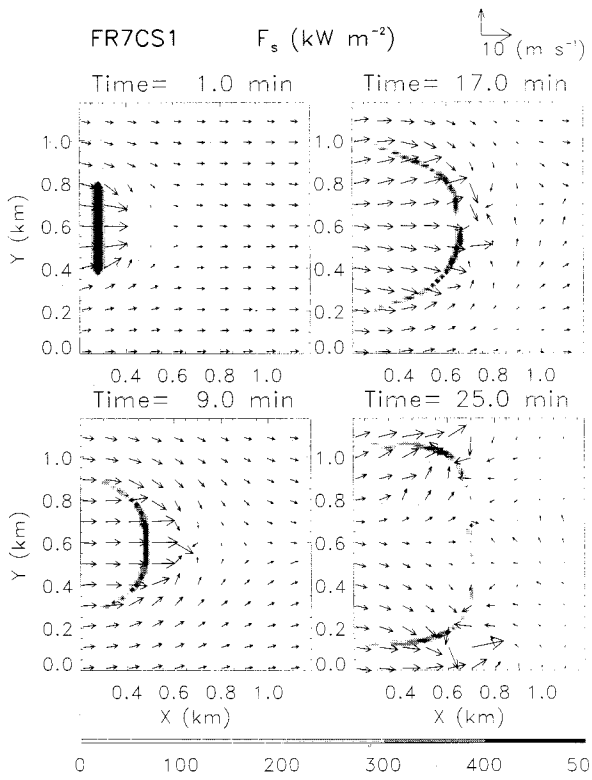

Figure 12. Four time levels of surface fuel ignition in a tanh profile ambient wind of $U_0 = 3$ m s^{-1} for FR7CS1. Shaded regions indicate fire fluxes in kW m^{-2}. The initial fire length is 420 m.

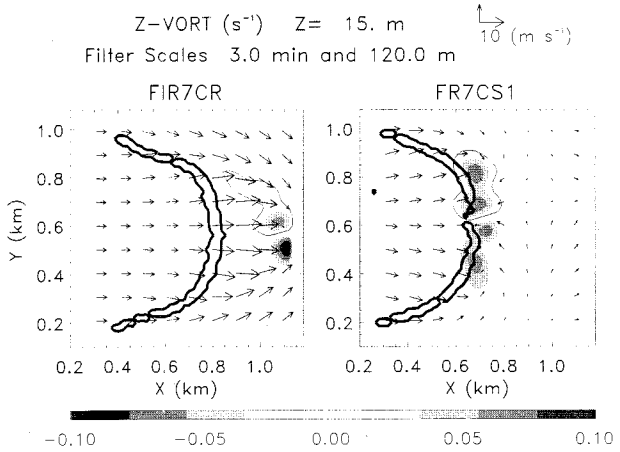

Figure 13. Vertical vorticity at $z = 15$ m AGL for (a) experiment FIR7CR and (b) experiment FR7CS1. Temporal averaging over a 3 min period, centered at $t = 18$ min, as well as spatial averaging over 120 m was applied to the model data to remove higher amplitude small fire line vortices.

For moderate ambient wind speeds, the coupled forest fire and atmospheric dynamics simulations show three basic mechanisms affecting fire line behavior. The first mechanism, discussed in Clark et al. (1996), is the effect of the near-surface convergence zone of the convection

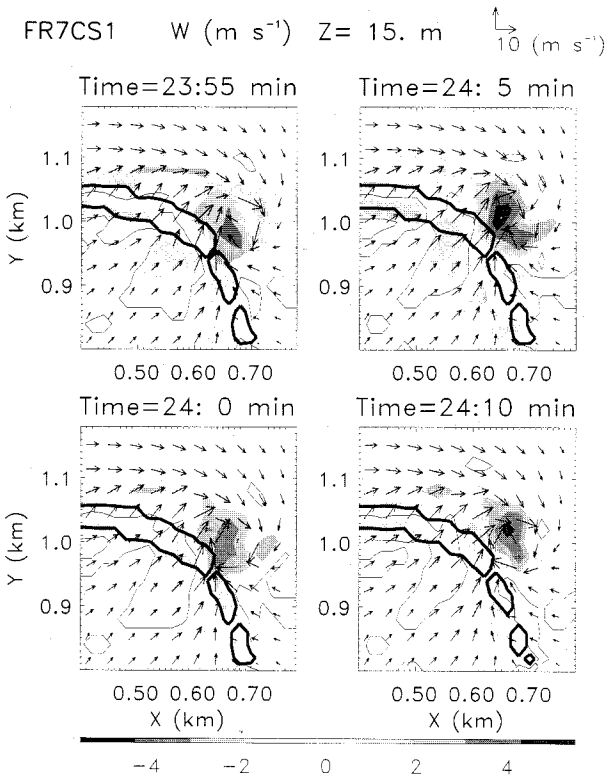

Figure 14. Four time levels of horizontal cross sections of $w(x,y)$ in m s^{-1} for the north-east region of experiment FR7CS1 (tanh profile ambient wind of $U_0 = 3$ m s^{-1}).

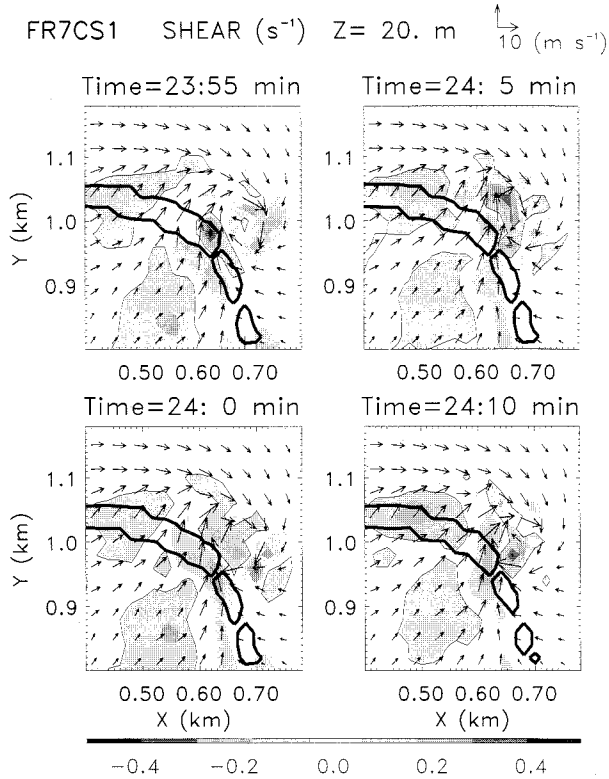

Figure 15. Same as Figure 14 except for the magnitude of the vertical wind shear $\partial|V|/\partial z$ in s^{-1}.

column inducing a parabolic or cone-like shape to the wind-driven line fire. This effect is seen in the early time history of all the wind-driven simulations with U_0 ranging from 2 to 5 m s^{-1}. The second mechanism is a longer term effect derived from the first, where the curved shape of the advancing fire front produces a vertically-oriented vortex pair situated in front of the fire. The third mechanism: in a case where the ambient wind reversed direction with height (experiment FR7CS1), this vortex pair eventually touched down in the fire, resulting in a break-up of the fire line into two distinct sections. In one other long term simulation where the wind speed remained constant at 3 m s^{-1} with height (experiment FIR7CR), the vortex pair touched down well in front of the fire line. In this case the fire line retained its curved shape throughout the 28 min of simulated time. The third mechanism is what we call "dynamic fingering", the result of vortex tilting at the small scales of the fire line. In this case the sense of vortex tilting amplifies the wind speed in the direction of fire spread resulting in a marked increase in the rate of spread. Experiment FR7CS1 presents a single event of dynamic fingering that resulted from the vertical tilting of a zone of negative shear (e.g., wind decreasing with height) produced by a fire-induced eddy at the fire front. The tilted zone of shear amplifies an existing vertical vortex to locally increase the rate of spread from 0.4 m s^{-1} to 0.9 m s^{-1}. We believe that this small-scale mechanism for

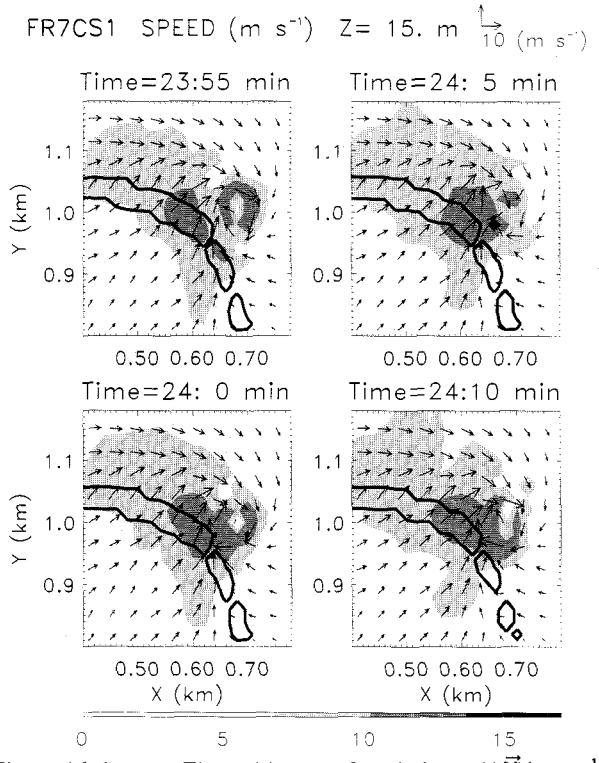

Figure 16. Same as Figure 14 except for wind speed $|\vec{V}|$ in m s^{-1}.

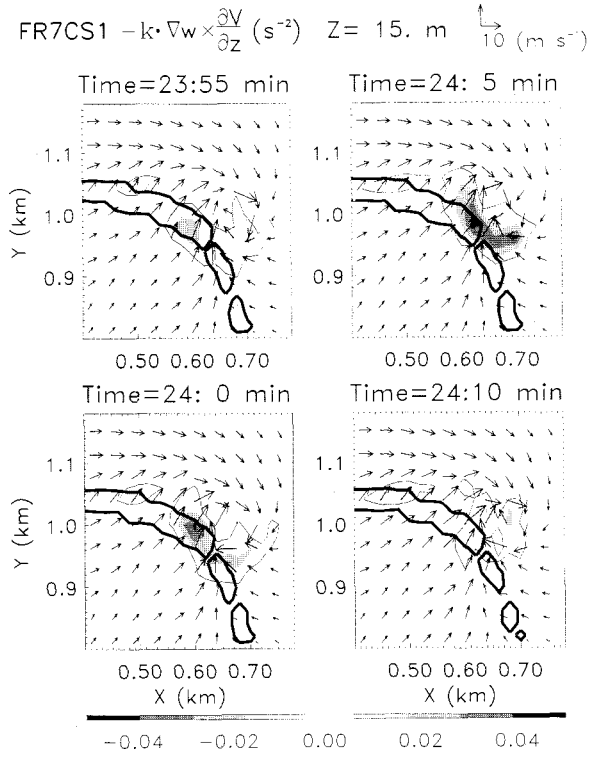

Figure 17. Same as Figure 14 except for the source of vertical vorticity due to vortex tilting of shear ($\frac{\partial \vec{V}}{\partial z}$) by the horizontal inhomogeneities in the vertical velocity field, w. Units are s^{-2}.

dynamic fingering may be basic to fire spread dynamics. It will be a topic of further investigations.

The dynamic fingering event is accompanied by a vertical vortex with an amplitude a little larger than 1 s^{-1}. This vertical vorticity is comparable to that of supercell tornadoes, approximately 0.3-1.2 s^{-1}, using tangential velocity and funnel width data of Bluestein et al. (1993). The updrafts associated with this vortex are as strong as 5 m s^{-1} at 15 m AGL. As these updrafts are sufficiently strong to loft burning material and cause spotting downwind of the fire, the results point to the possibility of introducing spotting in further model development. Another interesting feature of this intense vortex is the presence of multiple speed maxima. At 15 m AGL the analysis showed three local maxima of speed, indicating an unstable vortex. These vortices orbiting within a larger vortex resemble the subtornado-scale vortices called "suction vortices" that Fujita (1970,1971) identified as existing within a parent tornado. This phenomenon will be investigated further in the future.

Under special conditions this mechanism of dynamic fingering may also play a crucial role in a bifurcation of the fire dynamics leading to blowup fires. Both the duration and spatial extent of the amplification of the rate-of-fire spread could be significantly increased by the introduction of an external source of strong low-level negative wind shear, e.g., gust fronts or mountain valley flows. The continual forcing of dynamic fingering could then lead to rapid fire line spread resulting in a significant increase in the average rate of fire spread. An increase in spread-rate would then alter the energy balance such that the heat flux provided by the fire is sufficient to drive its own boundary layer circulation pattern and maintain the sheared ventilation pattern. The result is a bifurcation in the fire dynamics. Testing this hypothesis on the mechanism leading to blowup fires will be a topic of further investigation.

An important aspect of fire modeling is the simplification of the dynamic model for purposes of further idealized studies on fire line dynamics. Examples here might include development and testing of canopy drag formulations or the treatments of radiation. The current results indicate that all of the large F_c experiments would give equivalent results in two spatial dimensions. Thus a two-dimensional version of models such as this would be good test beds to efficiently develop and test model improvements.

Acknowledgments. We thank John Bally of the Bureau of Meteorology, Tasmania, for his assistance with the eucalyptus forest fuel model in this study. We are also indebted to Ian Knight, CSIRO, Canberra, for providing us with invaluable information on the behavior of short line fires. We also appreciate the reviews on the manuscript by Mitch

Moncrieff and Chris Davis.

References

Banta, R.M., L.D. Olivier, E.T. Holloway, R.A. Kropfli, B.W. Bartram, R.E. Cupp, and M.J. Post. 1992. Smoke column observations from two forest fires using Doppler lidar and Doppler radar. Journal of Applied Meteorology 31:1328-1349.

Blackadar, A.K. 1962. The vertical distribution of wind and turbulent exchange in a neutral atmosphere. Journal of Geophysical Research 67: 3095-3102.

Bluestein, H.B., J.G. LaDue, H. Stein, D. Speheger, and W. P. Unruh, 1993. Doppler radar wind spectra of supercell tornadoes. Monthly Weather Review 121:2200-2221.

Byram, G.M. 1954. Atmospheric conditions related to blowup fires. Station Paper No. 35. Southeastern Forest Experiment Station, Asheville, North Carolina.

Byram, G.M. 1973. Combustion of forest fuels. Forest Fire, Control and Use (edited by A. A. Brown and K. P. Davis), 2nd edition, McGraw-Hill, N.Y., 155-182.

Clark, T.L. 1979. Numerical simulations with a three-dimensional cloud model. lateral boundary condition experiments and multi-cellular severe storm simulations. Journal of the Atmospheric Sciences 36:2191-2215.

Clark, T.L., M.A. Jenkins, J. Coen and D. Packham, 1996. A coupled atmospheric-fire model: Convective feedback on fire line dynamics. Journal of Applied Meteorology 35:875-901.

Church, C.R., J.T. Snow, and J. Dessens. 1980. Intense atmospheric vortices associated with a 1000 Mw Fire. Bulletin of the American Meteorological Society 61:682-694.

Fujita, T.T. 1970. Lubbock tornadoes: A study of suction spots. Weatherwise 23:160-173.

Fujita, T.T. 1971. Proposed mechanism for suction spots accompanied by tornadoes. *Preprints, 7th Conference on Severe* Local Storms, Kansas City, American Meteorological Society, 208-213.

Grishin, A.M. 1992. Matematicheskoye modelirovaniye lesnykh pozharov i novyye sposoby bor'by s nimi (Mathematical modeling of forest firest and new methods of fighting them). Novosibirsk, "Nauka" Publishers, Siberian Division, 408 pp (Russian).

Heilman, W.E., and J.D. Fast. 1992. Simulations of horizontal roll vortex development above lines of extreme surface heating. International Journal of Wildland Fire 2:55-68.

Heilman, W.E. 1992. Atmospheric simulations of extreme surface heating episodes on simple hills. International Journal of Wildland Fire 2:99-114.

Kessler, E. 1969. On the distribution and continuity of water substance in atmospheric circulations. Meteorological Monographs No. 32, American Meteorology Society, 84 pp.

Lilly, D.K. 1962. On the numerical simulation of buoyant convection. Tellus 14:145-172.

Noble, I.R., G.A.V. Bary, and A.M. Gill. 1980. McArthur's fire-danger meters expressed as equations. Australian Journal of Ecology 5:201-203.

Rouse, H., W.D. Baines, and H.W. Humphreys. 1953. Free convection over parallel sources of heat. Proceedings of Physical Society, B, 393.

Schaefer, J.T. 1975. Nonlinear biconstituent diffusion: a possible trigger of convection. Journal of the Atmospheric Sciences 32:2278-2284.

Smagorinsky, J. 1963. General circulation experiments with the primitive equations. Proceedings of the International Symposium on Numerical Weather Prediction, Tokyo, Meteorological Society of Japan. pp 85-107.

Walker, J., 1981: Fuel dynamics in Australian vegetation. Fire in the australian biota. Edited by A.M. Gill, R.H.Groves, and I.R. Noble. Australian Academy of Science, 582 pages.

Wilhelmson, R.B., and J.B. Klemp. 1978. A numerical study of storm splitting that leads to long lived storms. Journal of the Atmospheric Sciences 35:1974-1986.